Journal of Power Sources 253 (2014) 315–331

Contents lists available at ScienceDirect

Journal of Power Sources

journal homepage: www.elsevier.com/locate/jpowsour

Review

Recent progress in the development of Li_2MnSiO_4 cathode materials

R.J. Gummow*, Y. He

School of Engineering and Physical Sciences, James Cook University, Townsville 4811, Australia

HIGHLIGHTS

- We review the published data on Li_2MnSiO_4 as a lithium-ion battery cathode.
- The various synthesis methods used for Li_2MnSiO_4 are examined.
- The structural form of the Li_2MnSiO_4 products is highlighted.
- The electrochemical performance of various Li_2MnSiO_4 samples is compared.
- Opportunities for future work are identified.

ARTICLE INFO

Article history:
Received 9 October 2013
Received in revised form
17 November 2013
Accepted 18 November 2013
Available online 5 January 2014

Keywords:
Lithium-ion battery
Cathode
Lithium manganese silicate
Capacity
Cell-cycling

ABSTRACT

Lithium ion batteries are under intense development to meet the performance specifications for consumer applications in portable electronic devices, electric vehicle batteries and stationary storage as back-up for intermittent renewable energy generation technologies. The most expensive and capacity-limiting component in these battery systems is the cathode material. Research has been directed to the development of novel cathode materials with high capacity and energy density and the lithium transition metal orthosilicates have been identified as possible high performance cathodes. In this review we focus on recent developments in the study of Li_2MnSiO_4 and its derivatives as a lithium-ion battery cathode material. Preparation techniques, structural issues, conductivity enhancement and complex morphologies are discussed, to show the recent improvements and limitations in synthesis and electrochemical performance.

1. Introduction

Sony released the first commercial lithium-ion battery in 1990 containing a carbon anode and a lithium cobalt oxide ($LiCoO_2$) cathode [1]. Since then research has been conducted to modify the cell components to improve both safety and electrochemical capacity, and to reduce cost. Much of the attention has focussed on the development of alternative cathode technologies, as the cathode capacity typically limits the cell capacity, and up to 40% of the cell cost is derived from the cost of cathode raw materials [2]. Due to market acceptance, lithium-ion batteries now dominate the portable electronics market. Concern for environmental protection, requiring reduction of green-house gas emissions, has led to new market opportunities for lithium-ion batteries. Large-scale applications, for instance, in electric vehicles to replace internal combustion engines, and as stand-by storage for intermittent renewable energy technologies like solar and wind power, have become the focus of lithium-ion battery developers. These applications place even more stringent performance requirements on batteries, and demand constant innovation in electrode materials [3,4].

The continuous development of Li-ion battery cathodes since the 1990's has been driven by the need to 1) maintain a high discharge voltage to maximize the energy density, 2) extend the useful range of lithium insertion and extraction to maximize capacity, and 3) improve safety by reducing the reactivity of cathodes in the charged state, while striving to use non-toxic and cheap materials to minimize environmental impact and cost. The drawback of lithium transition metal oxide cathodes, such as $LiCoO_2$, in lithium ion batteries is two-fold; firstly, the range of reversible lithium extraction and insertion is limited by safety and stability issues, leading to only moderate practical capacities [5] and secondly, the oxides are highly reactive and prone to O_2 release and potential thermal events when overcharged [6]. Considerable improvements in performance and safety have been achieved by

* Corresponding author. Tel.: +61 747816223; fax: +61 747816788.
E-mail addresses: Rosalind.gummow@jcu.edu.au (R.J. Gummow), yinghe.he@jcu.edu.au (Y. He).

0378-7753/$ – see front matter © 2013 Elsevier B.V. All rights reserved.
http://dx.doi.org/10.1016/j.jpowsour.2013.11.082

using mixed transition-metal oxides e.g. Co, Ni and Mn in the 1:1:1 atomic ratio to replace Co in $LiCoO_2$, but practical capacities remains limited to approximately 190 mAh g^{-1} [7,8].

Polyanionic compounds such as phosphates and silicates were proposed in 2002 as possible alternatives to lithium transition metal oxide cathodes [9]. This focus was motivated by the potential increased safety of these compounds compared to oxides, and the possibility of using cheaper, non-toxic metals such as Fe to replace Co and Ni. In the polyanionic units, the oxygen atoms are bound by strong, covalent bonds, reducing the risk of oxygen release in the charged state, and thus resulting in improved safety characteristics [10]. Polyanionic compounds also offer the advantage that the electrochemical properties can be adjusted by altering the nature of the X atom in the XO_4 polyanions [11].

$LiFePO_4$ is the most commercially successful polyanionic cathode material and was initially developed by Padhi and Goodenough in the 1990's [10,12]. $LiFePO_4$ has excellent rechargeability and safety characteristics and is made from cheap, non-toxic precursors. $LiFePO_4$ discharges through the $Fe^{2+/3+}$ redox couple on a flat voltage plateau at ~3.4 V with 95% of the theoretical capacity of 170 mAh g^{-1} [13]. The gravimetric energy density of $LiFePO_4$ (560 Wh kg^{-1}) is higher than that of $LiCoO_2$ (500 Wh kg^{-1}) but, due to the lower specific density of the material, the volumetric energy density is lower for $LiFePO_4$ (2000 Wh l^{-1}) compared to $LiCoO_2$ (2600 Wh l^{-1}) [13]. The drawback of the material is its poor intrinsic electronic conductivity, resulting in poor high current rate performance [14]. This limitation has been overcome by coating nanoparticles of active material with electrically conductive layers, for example carbon [15,16]. Excellent high rate performance of $LiFePO_4$ has also been reported by coating with amorphous $Li_4P_2O_7$ – like phases with enhanced ionic conductivity [17].

The lithium transition metal orthosilicates (Li_2MSiO_4, where M is a transition metal, for example, Fe, Co or Mn) were proposed as possible lithium-ion battery cathodes at the same time as the lithium transition metal phosphates [9]. In the orthosilicates, the lithium and transition metal cations are situated in tetrahedral sites in a distorted hexagonal-close-packed oxygen array. A detailed general review of the silicate family of cathode materials was published by Islam et al. in 2010 [18]. Li_2MnSiO_4 is the material in this family that offers the greatest promise to deliver high capacity, high energy density cathode materials. In this review we focus on Li_2MnSiO_4 and its derivatives with particular emphasis on the recent, advances that have been reported in the practical performance of these materials.

2. Lithium manganese orthosilicate (Li_2MnSiO_4)

Li_2MnSiO_4 first attracted the attention of cathode developers when it was suggested that both lithium ions in each formula unit could potentially be extracted at moderate voltages, resulting in a high theoretical capacity of 333 mAh g^{-1} [19,20]. This process potentially utilizes both the $Mn^{2+/3+}$ and $Mn^{3+/4+}$ electrochemical couples for the extraction of the 1st and 2nd lithium ions respectively. Although this is also theoretically possible for the Fe and Co analogues, in the case of Fe and Co, the $Fe^{3+/4+}$ and $Co^{3+/4+}$ couples are predicted to be outside the voltage stability window of common electrolytes [11]. The Ni analogue has not been synthesized experimentally but theory predicts prohibitively high voltages for lithium extraction from Li_2NiSiO_4.

2.1. Polymorphism and structural considerations

The transition metal orthosilicates are well-known to exhibit a wide variety of structural forms and Li_2MnSiO_4 is no exception. All four known ambient temperature polymorphs have Li, Mn and Si cations in tetrahedral co-ordination in a distorted hexagonally close-packed oxygen array and differ only in the arrangement of the tetrahedra. The structures can all be related to either the α or β-Li_3PO_4 structures [21]. The orthorhombic forms (*Pmn*2_1 and *Pmnb*) have two-dimensional pathways for Li-ion diffusion while the monoclinic forms (*P*2_1/*n* and *Pn*) are framework structures with Li-ion positions interconnected in three dimensions (Fig. 1). Other framework structures, such as the spinel structure of $Li_4Ti_5O_{12}$ are dimensionally stable when Li is inserted and extracted, which permits excellent reversibility, and makes it possible to utilize most of the theoretical capacity in practice [22]. Two-dimensional, layered structures such as the lithium transition metal oxides, however, tend to be destabilized when lithium is fully extracted and large dimensional changes result, leading to a limited range of lithium extraction in application and a reduction in the practical

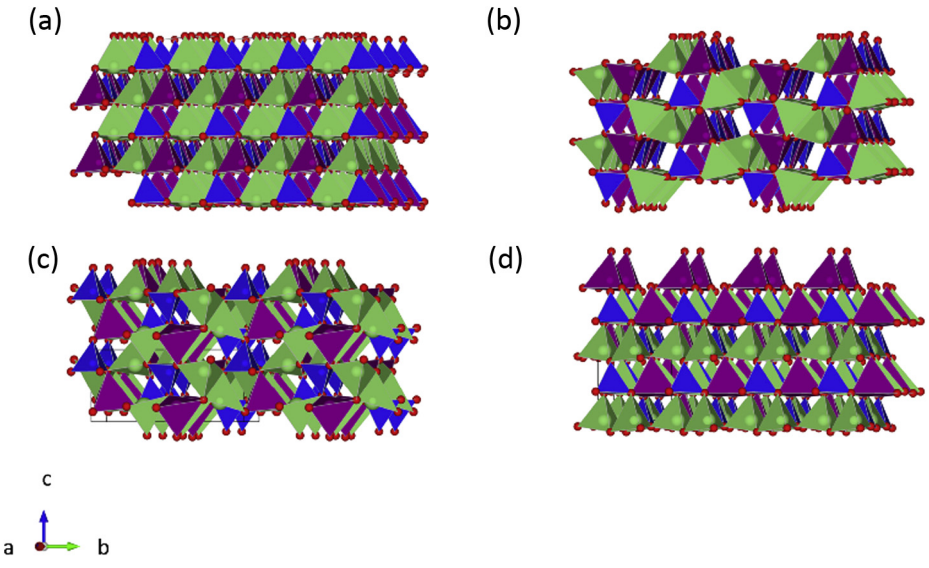

Fig. 1. Crystal structures of the four known ambient pressure polymorphs of Li_2MnSiO_4 (a) *Pmn*2_1 [19], (b) *Pmnb* [28], (c) *P*2_1/*n* [29] and (d) *Pn* [32]. Li tetrahedra are shown in green, Mn tetrahedra in purple and Si tetrahedra in blue, red spheres represent oxygen atoms. (For interpretation of the references to colour in this figure legend, the reader is referred to the web version of this article.)

capacity. It is clear, therefore, that various structural forms of Li_2MnSiO_4 will potentially have different electrochemical performance due to the variety of the pathways for lithium-ion diffusion through the crystal lattice [18] and the different interconnections of the Mn and Si tetrahedra. In the analogous case of Li_2FeSiO_4, clear differences in electrochemical properties have been demonstrated for three different structural forms prepared under different conditions [23].

The *Pmn*2$_1$ structural form of Li_2MnSiO_4, first reported by Dominko et al. [19], has a distorted orthorhombic crystal structure analogous to the Li_2FeSiO_4 structure reported by Nyten [24,25]. Synthesized products typically contain minor impurity phases of MnO and Li_2SiO_3. Initial Rietveld refinement of this structure showed that it has a high degree of disorder which includes both partial exchange of Li and Mn cations as well as partial migration of the Li, Mn and Si atoms into vicinal tetrahedral sites across the basal plane of the tetrahedra in the hexagonally close packed oxygen lattice [19]. This disorder is expected to be a disadvantage for Li-ion migration, as Mn ions in Li sites would block Li-ion diffusion pathways. More recent Rietveld refinement of high-quality single crystal XRD data for this polymorph, produced by hydrothermal synthesis, has shown that it gives a perfectly site-ordered structure for both Li and Mn [26]. An idealized crystal structure diagram of this polymorph of Li_2MnSiO_4 is shown in Fig. 1(a).

A second orthorhombic form with *Pmnb* symmetry was found, by theoretical calculations, to have very similar thermodynamic stability to the *Pmn*2$_1$ form, making it difficult to prepare in phase-pure form [27]. Recently, however, phase-pure *Pmnb* form Li_2MnSiO_4 has been prepared [28]. Rietveld refinement showed that this form showed no Li/Mn site/anti-site disorder potentially leading to good Li-ion diffusion properties.

The high temperature form of Li_2MnSiO_4 with monoclinic *P*2$_1$/*n* symmetry was first prepared by Politaev et al. at 1150 °C [29]. Subsequently other synthesis routes to this structural form were reported by Arroyo-de Dompablo et al. (sol–gel synthesis) [27] and Mali et al. (hydrothermal synthesis) [30]. Gummow et al. demonstrated that the *P*2$_1$/*n* polymorph could be stabilized by the partial substitution of Mn by Mg enabling synthesis of this form at temperatures of 700 °C [31]. Recently a novel fourth structural form of Li_2MnSiO_4, with monoclinic P_n symmetry, was prepared by ion-exchange from Na_2MnSiO_4 [32]. This polymorph was, however, unstable at elevated temperature and transformed to the orthorhombic *Pmn*2$_1$ form at 300 °C. Table 1 gives the space group and lattice constants for the known, ambient pressure, polymorphs of Li_2MnSiO_4 reported in the literature to date. Simulated reference XRD patterns (Cu Kα radiation) for the three polymorphs of Li_2MnSiO_4 that can be synthesized directly are given in Fig. 2. The XRD pattern of the P_n form was not included as the sample reported in Ref. [32] had a complex bimodal particle size distribution.

2.2. Electronic conductivity

The drawback of the lithium transition metal orthosilicate cathodes is their very low electronic conductivity since the MO_4 tetrahedra (where M = Fe, Mn or Co) are surrounded by insulating XO_4 tetrahedra (where X = Si in the case of the silicates) [27]. This feature is common to all polyanionic compounds including $LiFePO_4$, but the intrinsic conductivities of the silicates are significantly lower than the intrinsic conductivity of $LiFePO_4$ [33]. The electronic conductivities of Li_2FeSiO_4 and Li_2MnSiO_4 are of the order of 10^{-14} and 10^{-16} S cm^{-1} at room temperature [33,34], respectively. They both increase by two orders of magnitude at 60 °C. No significant difference in electronic conductivity of Li_2MnSiO_4 is anticipated for different structural forms, since isolated MnO_4 tetrahedra are present in all forms, and this is confirmed by the finding that calculated band gaps are very similar for different polymorphs [27]. Electronic conductivity can be enhanced by coating nanoparticles of active material with conductive layers, typically carbon. This strategy has been applied very successfully to $LiFePO_4$ and has also been used for Li_2MnSiO_4 (see Section 3).

Table 1
The space group and lattice constants of the known ambient pressure polymorphs of Li_2MnSiO_4 cathodes.

Space group	*a* (Å)	*b* (Å)	*c* (Å)	*β* (°)
*Pmn*2$_1$ [19]	6.3109(9)	5.3800(9)	4.9662(8)	/
*Pmn*2$_1$ [30]	6.2762(9)	5.3355(8)	4.9614(9)	/
Pmnb [30]	6.3148(1)	10.7742(5)	5.0138(2)	/
Pmnb [27]	6.30814(13)	10.75946(22)	5.00909(10)	/
Pmnb [28]	6.30694(3)	10.75355(4)	5.00863(2)	/
*P*2$_1$/*n* [29]	6.3368(1)	10.9146(2)	5.0730(1)	90.990
*P*2$_1$/*n* [31]	6.3435(4)	10.9208(7)	5.0818(5)	90.982(2)
P_n [32]	6.3368(1)	10.9146(2)	5.0730(1)	90.987(1)

2.3. Ionic conductivity

Although the electronic properties of the different polymorphs of Li_2MnSiO_4 are similar, the ionic conduction properties are expected to be significantly different due to the differences in the interconnection of lithium sites in different structural forms. Kuganathan et al. [35] calculated Li-ion diffusion pathways for the orthorhombic *Pmn*2$_1$ and monoclinic *P*2$_1$/*n* forms of Li_2MnSiO_4 and found that the barriers to Li-ion diffusion were lower in the *P*2$_1$/*n* form. Kuganathan et al. also demonstrated the curved, anisotropic pathways for lithium ion diffusion in Li_2MnSiO_4 polymorphs. Calculations by Fisher et al. [36] for all four ambient pressure polymorphs of Li_2MnSiO_4 confirm that all are poor conductors of Li-ions with strong anisotropy in conduction. Poor ionic conductivity is likely to limit high rate performance of Li_2MnSiO_4 cathodes.

3. Synthesis techniques and electrochemical performance

In this section the published studies of Li_2MnSiO_4 cathodes are reviewed. Table 2 gives a summary of the synthesis conditions, particle size, and carbon content and emphasizes the crystallographic structural forms of the Li_2MnSiO_4 samples reported in the literature. The phase purity and the degree to which the structure has been investigated are also highlighted to indicate areas where

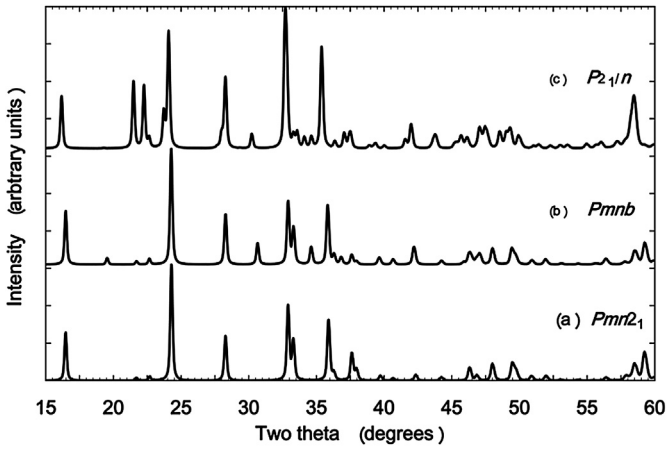

Fig. 2. Simulated XRD patterns (Cu Kα radiation) for the three polymorphs of Li_2MnSiO_4 that can be prepared directly. Crystallographic data for the simulations were taken from Refs. (a) [19], (b) [28] and (c) [29].

Table 2
Various synthesis techniques applied to Li_2MnSiO_4.

Ref.	Method	Comment on method	Precursors	Calcination conditions	Primary particle size (nm)	Carbon content (wt%)	Form and impurities
Dominko et al. [19]	Sol–gel Pechini synthesis	Produces small, uniform particles. Cost-saving and time-effective. Carbon-coating easily incorporated. Good control of stoichiometry and low content of impurities.	$Li(CH_3COO)\cdot 2H_2O$, $Mn(CH_3COO)_2\cdot 4H_2O$, nano-SiO_2, citric acid and EG. Si:citric acid:EG(6:1:3), stir 1 h maintain overnight, dry 60 °C 24 h	700 °C in Ar/5%H_2, 1–96 h	70	Not specified	$Pmn2_1$ + MnO (5.13%) + Li_2SiO_3 (0.46%)
Dominko et al. [20]			As in [19] but increased amount of complexation agent, amount not specified.	700 °C in high purity Ar for at least 1 h.	20–50	5 (TGA)	Not specified but XRD indicates $Pmn2_1$+ MnO
Dominko et al. [32]			As above but ratio of citric acid:EG:Si was 2:1:1 Modified Pechini: used $LiNO_3$ as Li-source and ratio of citric acid:EG:SiO_2 was 2:1:4	Temp not specified, Ar atmosphere Temp not specified, Ar/5% H_2	20–50 Not given	5 Not given	Not specified
Deng et al. [37]	Citric acid sol–gel	Particles are significantly larger than those from Pechini synthesis.	$Li(CH_3COO)\cdot 2H_2O$, $Mn(CH_3COO)_2\cdot 4H_2O$, citric acid and TEOS(ethanol solution). Reflux at 80 °C, 14 h. Heat to 75 °C to evaporate solvent, dry 100 °C overnight.	700 °C 12 h flowing Ar	200	10.5 (elemental analysis)	$Pmn2_1$ No MnO detected in XRD
Belharouak et al. [38]	Sol–gel	Particles are significantly larger than those from Pechini synthesis.	$Li(CH_3COO)\cdot 2H_2O$, $Mn(CH_3COO)_2.4\cdot H_2O$, $Si(CH_3COO)_4$ in acetic acid + cellulose as carbon source	600, 700 and 800 °C for 24 h under He/H_2 (3.5%)	200–300 as prepared	7	$Pmn2_1$ at 700 C with minor Mni_2SiO_3
Liu et al. [55]	Polyol	Fine particles achieved with excellent phase purity.	Li, Mn and Si acetates reflux in EG for 16 h at 196 °C, dry 150 °C, mill with sucrose	600 °C 10 h, inert atmosphere (not specified)	30	12.5 (elemental analysis)	$Pmn2_1$ – no impurities detected
Duncan et al. [31]	Sol–gel and ion exchange	Complex synthesis pathway. Difficult to incorporate carbon coating in the P_n form due to instability of the phase at high temperature.	Synthesis of Na_2MnSiO_4 from sodium acetate, Mn acetate TEOS and acetic acid, heated to 65 °C to dryness. Sucrose added to form carbon coat.	Calcined 500 C, 12 h, flowing Ar 5 wt% H_2. Ion-exchanged with LiBr.	>50 needle-like particles and <10 spherical particles		P_n form first report. Transforms to $Pmn2_1$ at 300 C.
Li et al. [36]	Solution Route	Produces good quality single-phase material. Small particles.	$Li(CH_3COO)\cdot 2H_2O$, $Mn(CH_3COO)_2\cdot 2H_2O$ and $Si(OC_2H_5)_4$ in a water–ethanol system. Stirred at 80 °C for 24 h under reflux, dried at 120 °C. Milled with sucrose in acetone	Pellets heated to 600 °C for 10 h in a flow of N_2.	20–30	9.1	$Pmn2_1$
Aravindan et al. [42]	Solid State synthesis	Very simple technique but the products require high temperature calcination and the particle size is large. Good control of stoichiometry. Extensive milling is needed to produce electrochemically active materials.	$LiOH\cdot H_2O$, SiO_2 and $MnCO_3$, 20 mol% adipic acid	900 °C in Ar	>500		Assigned to $Pmn2_1$ but some unidentified peaks
Gummow et al. [27]			$LiOH\cdot H_2O$, SiO_2 and $MnCO_3$, 20 mol% adipic acid	900 °C in Ar	>500		$Pmnb$ single phase, <1% MnO
Kojima et al. [47]	Molten carbonate flux	Low synthesis temperatures possible. Good control of stoichiometry. Particle size >100 nm.	$MnC_2O_4\cdot 2H_2O$ or $Mn(OH)_2$ with Li_2SiO_3 and $(Li_{0.435}\ Na_{0.315}K_{0.25})_2CO_3$ Added AB in ratio active:AB 5:4	CO_2/H_2 100:3 v/v at 500–650 °C CO_2/H_2 100:3 v/v at 700 °C, 2 h	Oxalate: 200–600 flakes Hydroxide:100–300 needles	40	$Pmn2_1$ Single phase
Mali et al. [29]	Hydrothermal	Requires the use of an autoclave for synthesis. Reduced synthesis temperatures	$MnCl_2\cdot H_2O$ + SiO_2 + $LiOH\cdot H_2O$, Teflon-lined SS autoclave, 10 bar Ar pressure, 6 h at 180 °C, wash with LiOH solution, dry 100 °C in Ar	400 °C in Ar 900 °C, 3 h, slow cooling in Ar 1 C/min		No carbon	$Pmn2_1$ + Li_2SiO_3 $Pmnb$ + Li_2SiO_3 + Mn_2SiO_4 $P2_1/n$ + Mn_2SiO_4

	are possible compared to other techniques.		900 °C, 6 h, quench to RT in Ar			
Manthiram et al. [44]	The use of microwave heating reduces synthesis time. Fine particles achieved. Very high pressure.	TEOS, LiOH, $Mn(CH_3COO)_2 \cdot 4H_2O$ dissolved in TEG, placed in a quartz vessel, microwave at 600 W for 25 min ($T = 300$ C, $P = 30$ b), wash with acetone, add 30 wt% sucrose	650 °C 6 h in Ar	20 nm agglomerated	12% TGA	Assigned to $P2_1$ but no refinement
Aravindan et al. [46]	Complex morphology	$LiOH \cdot H_2O$ + SiO_2 + $MnCl_2 \cdot 4H_2O$ + EG, Teflon lined SS autoclave, 150 °C for 48 h, dried 60 °C overnight. Mixed with adipic acid.	700 °C in Ar	Flower-like, agglomerates of ~30 nm primary particles		As prepared: $Pmn2_1$ with Li_2SiO_3 impurity Calcined after C addition: $Pmn2_1$ with minor MnO.
Kuezma et al. [45]		$LiOH \cdot H_2O$ (in excess) + $Mn(CH_3COO)_2 \cdot 4H_2O$ + TEOS + urea Autoclave at ambient pressure, 1000 W, 2 h at 260 °C. Dried 60 °C overnight. Added GA + citric acid	5 °C min^{-1} to 700 °C for 5 h	Carbon-coated particles are densely packed 15–100nm	LMS-1CA 10.5% LMS-5CA 31.7%	As prepared: assigned to $Pmn2_1$ Calcined after C addition: assigned to $P2_1/n$ but characteristic reflections absent, no refinement.
Kempaiah et al. [48]	Supercrtitcal conditions with very high pressures requiring specialized equipment. Very short reaction time. Extremely small particles.	$MnCl_2 \cdot 4H_2O$ + TEOS + LiOH + ascorbic acid reducing agent in ethanol+H_2O solution. Batch reactors at 300 °C and 38 MPa for 5 min. Quenched. Coated with 20 wt% PEDOT.	Heated to 300 °C in Ar/H_2	5–20 nm (TEM) 18 nm (Scherrer)	13.3% TGA	$Pmn2_1$ well-defined, no impurities
Rangappa et al. [50]	As above. Nanosheet morphology achieved. Difficulty in producing phase-pure material.	$MnCl_2 \cdot 4H_2O$ (0.1 mmol) and TEOS in 15 ml ethanol at 50 °C. Solutions of $LiOH \cdot H_2O$ (0.4 mmol) and ascorbic acid (0.1 mol) in 5 ml water. Solutions mixed with stirring over 1 h. 5 ml of precursor solution in 10 cc3 volume stainless steel reactor and heated up to 350–420 °C at a pressure of 38 MPa for 4–10 min. Quenched, dried in vac at 120 °C for 12 h. Milled with PEDOT (10 wt%) and MWCNT (5 wt%) at 300 rpm for 12 h.	300 °C for 4 h in Ar	Nanosheets a few atoms thick and 150–300 nm wide	Not given	Assigned to $P2_1/n$ but characteristic reflections absent, no refinement. Major unidentified impurities.
Devaraju et al. [51]	As above. The use of surfactants results in complex particle morphologies.	$MnCl_2 \cdot 4H_2O$ was dissolved in a mixed solution of water and DEG with constant stirring, followed by addition of TEOS and LiOH. The solution mixture and oleic acid or oleylamine were transferred to high pressure batch reactors (10 ml), heated at a high pressure (38 MPa) to 400 °C for 4 min. Quenched. Milled with (PEDOT, 10 wt%) and carbon black (10 wt%)	Dried at 450 °C 5 h in reducing atmosphere.			
		a) Water + DEG + oleic acid 400 C for 4 min b) 400 C for 4 min with increased amount of oleic acid. c) 1) 15–20 nm particles 2) 30–50 nm particles 3) 50–70 nm particles 4) 70–100 nm particles		a) Mono-disperse <5 nm b) 200–400 nm flowers, 4–5 nm nano-particles c) Spherical particles	a) 18 b) 24 c) 1) Not given 2) 20 3) Not given 4) Not given	a) $Pmn2_1$ with Li_2SiO_3 no refinement b) $Pmn2_1$ no refinement c)1) Not given 2) Major MnO impurity 3) Major MnO impurity 4) Major MnO impurity

(continued on next page)

Table 2 (*continued*)

Ref.	Method	Comment on method	Precursors	Calcination conditions	Primary particle size (nm)	Carbon content (wt%)	Form and impurities
Shao et al. [56]	Spray pyrolysis and wet ball milling	Low synthesis temperature, fine particles.	$LiNO_3$, $Mn(NO_3)_2{\cdot}6H_2O$, $Fe(NO_3)_3{\cdot}9H_2O$ and TEOS in distilled water + droplets of HNO_3 to hydrolyse TEOS. Atomized at.7 MHz in an ultrasonic nebulizer. Spray pyrolysis with N_2 carrier gas (2 dm^3 min^{-1}), heated 400 °C. Wet ball mill 8 h with 20 wt% AB.	600 °C in N_2	65	20	$Pmn2_1$

further structural studies are needed to clarify the nature of the electrochemically active species. Table 3 summarizes the electrochemical testing parameters recorded, to enable direct comparison of the performance of samples prepared and tested under various conditions. Figures that show the electrochemical charge/discharge profiles have been included in the text to illustrate, not only the capacities achieved, but also the voltage profiles and polarization. Practical application of cathode materials requires high energy density determined by both high capacity and high voltage over the discharge cycle. In the comparison of the electrochemical performance of various Li_2MnSiO_4 samples, the capacity recorded above 2.5 V has been quoted to illustrate that, in several cases, although very high discharge capacities are reported, much of this capacity is at a low voltage resulting in cathodes with a low overall energy density.

3.1. Sol–gel synthesis and the $Pmn2_1$ structural form

In early studies, Dominko and co-workers aimed to optimize the performance of Li_2MnSiO_4 by minimizing the particle size and coating the particles with a conductive carbon layer [19,20,33], following the success of this strategy in optimizing the electrochemical performance of $LiFePO_4$. Dominko et al. [19] used a modified Pechini sol–gel synthesis route to form the $Pmn2_1$ orthorhombic form of Li_2MnSiO_4 (94.42 wt.%) with minor impurities of MnO (5.13 wt.%) and Li_2SiO_3 (0.46 wt.%). Primary particles were approximately 70 nm in diameter with islands of amorphous carbon particles between them, but no clearly defined nano-layer of carbon on the particle surface. When these materials were tested as cathodes in lithium cells only 0.6 of the Li ions in the material were utilized reversibly on the first cycle and the reversible capacity faded rapidly to only 0.3Li ions on the 3rd cycle (Fig. 3). The poor performance was attributed to both imperfect electronic wiring due to the lack of a discrete carbon coating, and also to the need for electrolytes stable well above 4.5 V to allow full extraction of Li on charge.

In a subsequent study by the same authors [20], an increase in the amount of the complexing agent resulted in smaller particles (20–50 nm) with a uniformly distributed carbon content of ~5 wt.%. Electrochemical evaluation was performed using cathodes of active material and an electrolyte based on LIBOB salt with an upper voltage cut-off of 4.2 V to minimize the risk of electrolyte decomposition on charge. Room temperature cycling results were, however, comparable to those of the earlier study [19]. To explore the performance at elevated temperature, cells were cycled at 60 °C and gave an initial lithium extraction plateau near 4 V with a capacity corresponding to the extraction of 1.5Li ions per formula unit, but this capacity was not reversible on discharge or on subsequent cycles. It was stated that it was not clear if the large capacity was due only to lithium extraction, or if there was some degree of irreversible electrolyte interaction with the active material that contributed to the observed capacity. Even after ball-milling to improve the distribution of components, and the contact between them, the improvement in capacity was small and the polarization was only reduced by about 20 mV. All samples showed a rapid loss of capacity with charge–discharge cycling corresponding to a 40 mAh g^{-1} loss after 10 cycles.

The authors stated that despite adopting the same strategy of particle size reduction and carbon coating used successfully to activate $LiFePO_4$, the performance of Li_2MnSiO_4 cathodes remained surprisingly poor and cells showed rapid capacity fade with cycling. In order to understand this, ex-situ XRD studies of partially charged cathode samples were performed. The results showed no significant change in peak position with changes in Li content, but a

Table 3
Summary of electrochemical performance of Li_2MnSiO_4.

Reference	Method	Electrode formulation	Electrolyte	Voltage limits (V)	Current rates	Capacity (mAh g^{-1})		Comments
Dominko et al. [19,20]	Sol-gel	Active material: Teflon binder: carbon black 85:7:8	1 M $LiPF_6$ in EC:DEC 1:1	2–4.5	C/30		D1: 100 D5: 50	
Dominko et al. [20]		Active material: carbon:PVDF 80:10:10	0.8 M LiBOB in EC:DEC (1:1 by volume)	2–4.2	C/20	RT: D1: 16 60 °C: D1: 100 Li's		
Dominko et al. [33]		Active material + 10% AB, no binder	0.8 M LiBOB in EC:DEC (1:1 by volume)	2–4.2 2–4.5 2–4.2	C/20 C/20 C/100	C1: 232 C1: 310 C1: 299	D1: 140 D1: 150 D1: 132	Large charge capacity not recovered on discharge
Deng et al. [38]		Active material: carbon black:PVDF 80:10:10	1 M $LiPF_6$ in EC:DMC	1.5–4.8	10 mAh g^{-1} (~C/16)	C1: 200 C5: 120 C10: 100	D1: 140 D5: 100 D10: 85	<1 e capacity
Belharouak et al. [39]		Active:AB:PVDF 75:15:10	1.2 M $LiPF_6$ in 3:7 v/v EC:EMC	1.5–4.8	10 mAh g^{-1} (~C/16)	Coated: C1: 190 C5: 140 C10: 125 Milled: C1: 175 C5: 125 C10: 105	 D1: 135 D5: 130 D10: 120 D1: 115 D5: 120 D10: 100	
Liu et al. [55]		Active:C:PVdF 80:10:10	1 M $LiPF_6$ in 1:1 v/v EC:DMC	1.5–4.8	C/30 0.1 C 0.5C	C1: 219	D1: 132 D10: 108 D1: 126 D10: 87 D1: 105 D10: 72	
Duncan et al. [32]		Active:Super S:graphite:PVDF 80:5:5:10	1 M $LiPF_6$ in 3:7 EC:DEC	1.8–4.6	Not given	P_n: C1: 100 $Pmn2_1$: C1: 120	 D1: 120 D5: 110 D10: 100 D1: 105 D5: 100 D10: 97	Very similar performance for two different polymorphs.
Li et al. [37]	Solution	Active:C:PVDF 80:10:10	1 M LiPF6/EC-DMC 1:1 wt%	1.5–4.8	5 mA g^{-1} 30 mA g^{-1} 150 mA g^{-1}		D1: 210 D5: 170 D10: 140 D1: 180 D1: 135	1st report of >1 e capacity on discharge Capacity loss due to amorphization
Aravindan et al. [42]	Solid state	Active:ketjen black :TAB 12:11:3	1 M $LiPF_6$ in EC:DMC 1:1 v/v	1.5–4.8	C/20	As-prepared: C1: 97 C5: 50 Heat treated: C1: 110 C5: 105 C10: 105	 D1: 45 D5: 30 D1: 100 D5: 100 D10: 100	Steep discharge curves with no plateau region Very high carbon content
Kojima et al. [47]	Molten carbonate flux	Active/C mixture: AB:PTFE 80:13:7	1 M LiPF6 in EC/DMC 1:1 v/v	1.5–4.5	10 mA g^{-1}	Samples from hydroxides: C1: 170 C2: 160 C5: 145 D10: 120	 D1: 155 D1: 150 D5: 135	Good plateau, low polarization, 40% C in sample
Manthiram et al. [44]	Hydrothermal	Active:C:PTFE 75:20:5	1 M $LiPF_6$/EC-DMC 1:1	1.5–4.7	C/20[a]	Room temperature: C1: 280[b] C2: 250 55 °C: C1: 340 C2: 260	 D1: 210 D2: 200 D10: 150 D1: 245 D2: 220 D10: 65	>1 e capacity 150 mAh g^{-1} above 2.5 V at room temperature for D1 Very rapid decay of capacity at 55 °C
Aravindan et al. [46]		Active:ketjen black :TAB 12:11:3	1 M $LiPF_6$ in EC:DMC 1:1 v/v	1.5–4.8	C/20	As-prepared : C1: 97 C5: 50 Heat treated: C1: 110 C5: 105 C10: 105	 D1: 45 D5: 30 D1: 100 D5: 100 D10: 100	Steep discharge curves with no plateau region. Very high carbon content.
Kuezma et al. [45]		Active:AB:PVDF 75:15:10	1 M LiBOB in EC:DEC 1:1 v/v	2.0–4.5	C/10	Room temp: C1: 75 C3: 200	 D1: 130 D3: 170	Rapid capacity loss at 50 °C after 3 cycles

(*continued on next page*)

Table 3 (*continued*)

Reference	Method	Electrode formulation	Electrolyte	Voltage limits (V)	Current rates	Capacity (mAh g^{-1})		Comments
						50 °C C1: 250 D1: 250 C3: 250	D3: 250	
	D5: 65							
Kempaiah et al. [48]		PEDOT coated active:AB:PTFE 83:10:7	1 M $LiClO_4$ EC:DEC 1/1 v/v	1.5–4.5	C/20	Room temp: C1: 280	D1: 280 D2: 200 D5: 180 D20: 140	Steep discharge curves. No plateau region. Most capacity below 2.5 V
						40 °C C1: 300 C2: 290	D1: 300 D2: 280 D5: 275 D20: 230	
Rangappa et al. [50]		PEDOT coated active:AB:PTFE 85:10:5	1 M $LiClO_4$ EC:DEC 1/1 v/v	1.5–4.8	C/50	Room temp: C1: 150 C2: 190	D1: 130 D2: 210	Only 75 mAh g^{-1} above 2.5 V at room temp.
						45 °C C1: 350 C2: 350	D1: 350 D2: 350 D10: 300 D20: 300	Rapid decay in capacity after 20 cycles
Devaraju et al. [51]		PEDOT coated active material (10 wt.%): carbon: PTFE	1 M $LiClO_4$ in EC/DEC 1/1 v/v	1.5–4.8	0.05C			2-step discharge
		a) Monodisperse nanoparticles 75:18:7				a) C1: 300 C3: 200 C5: 190	D1: 300 D3: 200 D5: 190	~140 mAh g^{-1} above 2.5 V on D1
		b) 30–50 nm sized particles 73:20:7				b) C1: 300 C3: 300 C5: 300	D1: 225 D3: 175 D5: 170	~125 mAh g^{-1} above 2.5 V on D1
		c) Hierarchical nanostructures 69:24:7				c) C1: 300 C3: 300	D1: 280 D3: 250	~75 mAh g^{-1} above 2.5 V on D1
						C5: 300	D5: 240	
Shao et al. [56]	Spray pyrolysis and wet ball-milling	Active:PVDF:AB 70:10:20	1 M $LiPF_6$ in 1:1:v/v EC:DMC	1.5–4.8	0.05C = C/20	C1: 325	D1: 200	Amorphization confirmed on the 1st charge to 4.8 V.
					0.1C = C/10	C1: 275 D5: 140	D1: 185 D10: 120	Poor capacity retention with cycling.
					1C	C1: 175 D5: 100	D1: 125 D10: 80	

[a] For C-rate calculations 1C = 167 mA g^{-1}.
[b] C1 = capacity on the 1st charge cycle, D1 = capacity on 1st discharge cycle.

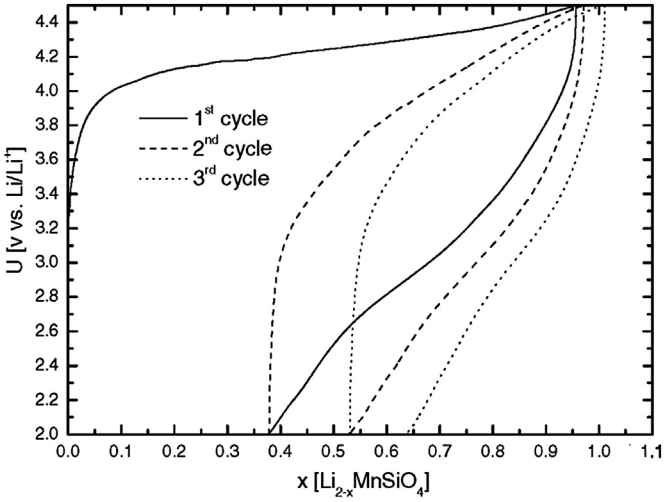

Fig. 3. Voltage profiles of Li_2MnSiO_4 cycled at room temperature and at a rate of C/30. Reprinted from Ref. [19] copyright (2006), with permission from Elsevier.

gradual loss of X-ray peak intensity was observed as the degree of Li extraction increased, with virtually no peaks visible for $x > 1$ in $Li_{2-x}MnSiO_4$ and no recovery of peaks after the 1st discharge cycle (Fig. 4) [20]. This indicated significant, irreversible structural change when Li was extracted on the 1st charge cycle but it was noted that, even after the loss of crystallinity, the product continued to cycle with a capacity greater than 100 mAh g^{-1}. These results were confirmed by the parallel study of Li et al. [37] and subsequent in-situ studies by Dominko et al. [33].

The tendency for the structure of $Li_{2-x}MnSiO_4$ to collapse when Li was extracted was investigated using DFT simulations by Kokalj et al. [34]. It was found that the volume of the crystal lattice varied very little for $0 \leq x \leq 1$ (less than 2%) but dropped dramatically for $x > 1$ with a ΔV of −17 and −27% for $Li_{0.5}MnSiO_4$ and $MnSiO_4$, respectively. This finding was taken as a clear indication of structural collapse for $x > 1$, in agreement with the findings of Dominko et al. [20] and Li et al. [37]. TEM observations of partially charged cathodes indicated some particles that were crystalline and some particles that were amorphous and this was interpreted as evidence for a phase separation mechanism for Li extraction as found in $LiFePO_4$ [34].

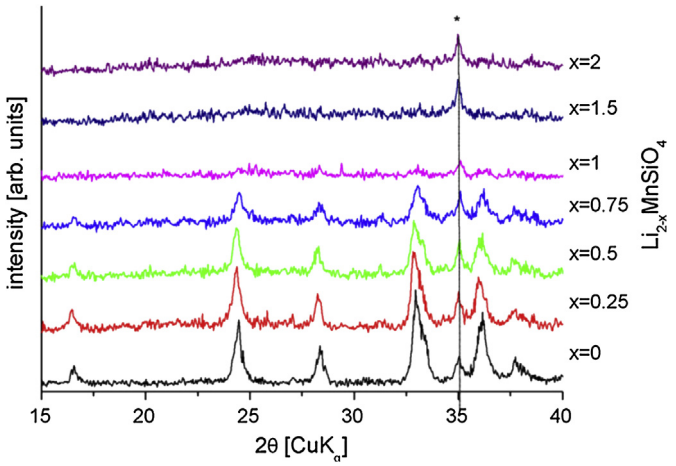

Fig. 4. X-ray diffraction patterns of compositions obtained with electrochemical oxidation of Li_2MnSiO_4-based composites. The value of *x* corresponds to expected chemical composition of the electrode that is based on the amount of charge passed through the cell. The remaining diffraction peak marked with asterisk denotes MnO impurity.
Reprinted from Ref. [20] copyright (2007), with permission from Elsevier.

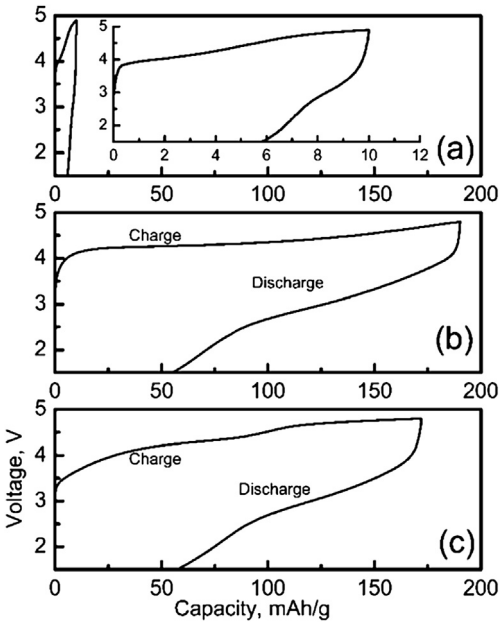

Fig. 5. Voltage profiles of (a) as-prepared Li_2MnSiO_4, (b) carbon-coated Li_2MnSiO_4, and (c) high-energy ball-milled Li_2MnSiO_4.
Reprinted with permission from Ref. [39] copyright (2009) American Chemical Society.

Deng et al. [38] published a study of Li_2MnSiO_4 prepared by sol–gel synthesis using TEOS as the SiO_2 source and calcined in flowing Ar at 700 °C. The product was indexed with the orthorhombic $Pmn2_1$ space group; although no detailed structural analysis was undertaken. The grain size was approximately 50 nm. The initial discharge capacity was approximately 145 mAh g^{-1} and dropped off rapidly with cycling. The cycling results confirmed the earlier findings of Dominko et al. [20] despite the significantly higher charge cut-off voltage of 4.8 V.

Belharouak et al. [39] prepared Li_2MnSiO_4 by a sol–gel route using Li, Mn and Si acetates in acetic acid to form a gel product. After drying at 100 °C, the gel was heated to 600, 700 and 800 °C for 24 h under He/H_2 (3.5 vol.%) gas flow. Cellulose was added to the reaction mixture as a carbon source leading to a final carbon content of 7 wt.% in the products. The optimum synthesis temperature to minimize impurities and produce $Pmn2_1$ form Li_2MnSiO_4 was found to be 700 °C. Samples consisted of micron sized aggregates of 100–200 nm primary particles after preparation and samples were milled for 4 h in a ball-mill to reduce the size of the particles and improve electrochemical activity. While the as-prepared sample showed very poor electrochemical performance, the carbon-coated and ball-milled samples showed improved performance of 190 and 135 mAh g^{-1} and 172 and 155 mAh g^{-1} for the first charge and discharge capacities respectively (Fig. 5). Once again rapid capacity fade with cycling was observed and, after 15 cycles, only 98 and 79 mAh g^{-1} discharge capacity was retained for the carbon-coated and ball-milled samples respectively.

A similar study using adipic acid as the carbon source was published by Aravindan et al. [40] with dispersed 25–30 nm particles of Li_2MnSiO_4 and residual carbon from the synthesis. The initial discharge capacities reported were 161 mAh g^{-1}, dropping to 120 mAh g^{-1} after 50 cycles, with steeply sloping discharge curves over the entire voltage range of 1.5–4.8 V.

In 2009 Dominko et al. [41] performed an in-situ XAS study to examine the oxidation state of Mn as a function of state of charge (orthorhombic $Pmn2_1$ structural form 83 wt.%, 15 wt.% MnO and 1.9 wt.% Li_2SiO_3). In-situ XANES measurements showed that, at 4.5 V, only 60% of the Mn^{2+} had been oxidized to Mn^{3+}, that is, only 0.6Li's had been extracted from the structure. After discharging, all the Mn was found to be in the 2+ state, as found for the starting material, but XAFS measurements indicated that the local environment around the Mn cations was not completely reversible with cycling implying some irreversible structural change. The authors therefore found no evidence for >1Li extraction on charge and confirmed that some alteration in the crystal structure occurred when the sample was charged.

In summary, results from this series of studies show that, despite the high theoretical capacities predicted, orthorhombic Li_2MnSiO_4 with the $Pmn2_1$ structural form, did not perform as hoped. Initially this was believed to be due to the very low electronic conductivity of the material. This explanation was soon dismissed, however, as, even after reduction of particle sizes to the range of 20–30 nm, and coating with carbon, the electrochemical performance remained disappointing. In fact, XAS results indicated that <1Li was extracted from Li_2MnSiO_4 on charge, and the intensities of X-ray diffraction peaks dropped off rapidly when samples were delithiated electrochemically. This evidence of dramatic structural change was confirmed by evidence of a change in crystallographic environment around the metal cations after cycling given by both NMR and EXAFS data.

3.2. Ion exchange and the P_n structural form

In 2011 Duncan et al. [32] used an ion-exchange route to prepare the novel monoclinic P_n form of Li_2MnSiO_4. The motivation for this study was the hope that the monoclinic form, with its three-dimensional framework structure, would be more stable to lithium extraction than the two-dimensional orthorhombic $Pmn2_1$ structure examined in earlier studies. The P_n form of Li_2MnSiO_4 was found to be metastable, transforming to the $Pmn2_1$ form when heated at 300 °C, preventing conventional carbon-coating. The electrochemical cycling results for the P_n form were very similar to those of the well-known $Pmn2_1$ form (Fig. 6). Capacity fade was comparable for both forms, with 65 and 70 mAh g^{-1} for the *Pn* and $Pmn2_1$ forms respectively after 50 cycles. This was contrary to the expectation that, when Li is extracted, the framework structure of the delithiated P_n form would be more stable than the delithiated, layered $Pmn2_1$ form.

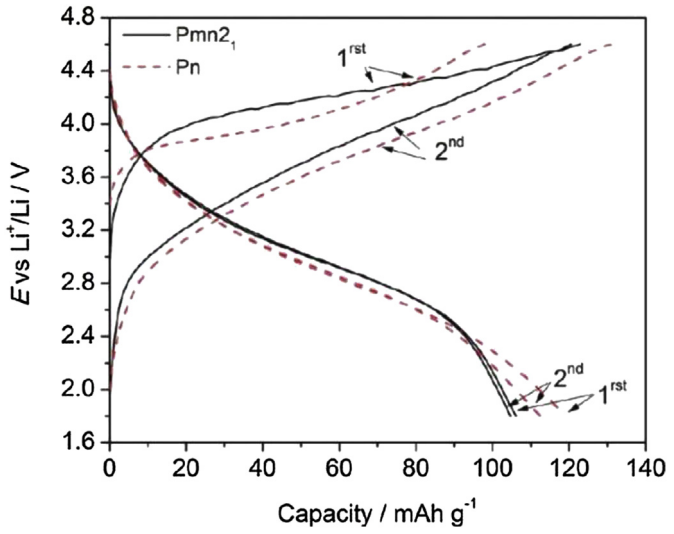

Fig. 6. Charge–discharge profile of $Pmn2_1$ (black line) and *Pn* (red dashed line) Li_2MnSiO_4. (For interpretation of the references to colour in this figure legend, the reader is referred to the web version of this article.)
Reprinted with permission from Ref. [32] Copyright (2011) American Chemical Society.

3.3. Solid state synthesis and the Pmnb form

Solid state synthesis was used by Aravindan et al. [42] to produce Li_2MnSiO_4 from $LiOH{\cdot}H_2O$, SiO_2 and $MnCO_3$ precursors with 20 mol% adipic acid as carbon additive and calcination at 900 °C in Ar. Particles were large (>0.5 μm) as typically found for this solid state technique. It was shown that, when the carbon content in the cathode mix was increased to 42% of the cathode mass, a reversible capacity of approximately 130 mAh g^{-1} was achieved and retained for 40 cycles. The good reversibility was attributed to retention of the crystal structure with cycling.

It is worth noting that, in the light of the current knowledge of the different polymorphs of Li_2MnSiO_4, there appear to be some inconsistencies in the interpretation of the XRD data reported in this paper. While no detailed structural analysis of the product was performed, the product was indexed to the $Pmn2_1$ structural form of Li_2MnSiO_4, with minor impurities of MnO and Li_2SiO_3. There was, however, a significant peak at 31° 2θ (Cu Kα radiation) in the XRD spectrum of the product, inconsistent with the $Pmn2_1$ structural form. In addition, no detailed analysis of the XRD pattern of the cycled product was performed, so the claim that the good cycling performance of the product was due to retention of the structure with cycling, cannot be substantiated. Further, the shape of the discharge curves for the samples with high carbon content also only showed about 80 mAh g^{-1} capacity above 2.5 V with a small plateau at 4.3 V followed by a steeply sloping voltage curve over the rest of the capacity range (Fig. 7).

A subsequent study by Gummow et al. [28] showed, with simultaneous Rietveld refinement of neutron and XRD data, that a product produced by solid state synthesis under the same conditions used by Aravindan et al. [42] was in fact single-phase, *Pmnb* form Li_2MnSiO_4 with the characteristic identifying peak at 31° 2θ (Cu Kα radiation). This study demonstrated that the *Pmnb* form had limited electrochemical activity due to the large particle size of the product (50 μm). In a subsequent study of ball-milled *Pmnb* material [43], an initial discharge capacity of 113 mAh g^{-1} was obtained for the *Pmnb* form, and, although the capacity dropped off rapidly initially, the introduction of a constant voltage hold at the end of the charge cycle improved the capacity retention somewhat. The shape of the discharge curves was steeply sloping with no well-defined plateau. Selected area electron diffraction data (SAED) of charged cathodes showed that some particles of charged material retained their crystallinity while other particles amorphized [43] as seen earlier for the $Pmn2_1$ form by other investigators [34].

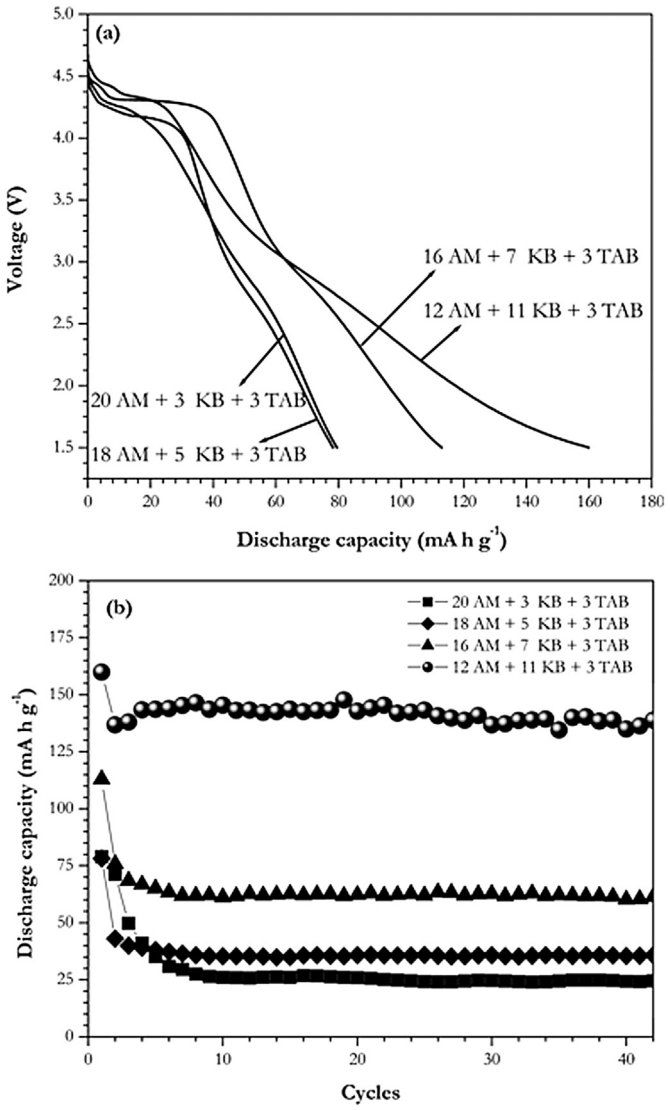

Fig. 7. Electrochemical performance of Li/Li_2MnSiO_4 cells at room temperature conditions, (a) initial discharge traces of Li/Li_2MnSiO_4 cells containing various amounts of carbon and (b) cycling profiles of Li/Li_2MnSiO_4 cells comprising different ratios of carbon (AM: active material (Li_2MnSiO_4), KB: ketjen black, TAB: teflonized acetylene black).
Reprinted from Ref. [42] with permission of The Royal Society of Chemistry.

3.4. Mg substitution and the $P2_1/n$ monoclinic structural form

As stated earlier, the monoclinic forms of Li_2MnSiO_4 are expected to have different electrochemical properties compared to the orthorhombic forms. The $P2_1/n$ form of Li_2MnSiO_4 was first prepared by Politaev et al. [29] by solid state synthesis at 1150 °C in Ar atmosphere. Initial electrochemical evaluation of this polymorph showed that it was essentially electrochemically inactive. This result is not surprising considering that the particles were large, as a result of the high synthesis temperature, and the fact that no carbon additives were included in the synthesis.

Gummow et al. [31] showed that partial Mg substitution for Mn in Li_2MnSiO_4 led to stabilization of the $P2_1/n$ form at lower temperatures than for unsubstituted Li_2MnSiO_4. When 40 or 50% of the Mn was substituted with Mg, the $P2_1/n$ structural form could be prepared at a calcination temperature of only 700 °C by solid state synthesis. The electrochemical activity of the $P2_1/n$ form was demonstrated in this study although the physical form of the product was still not ideal for optimum electrochemical performance.

3.5. Hydrothermal synthesis

Hydrothermal synthesis of Li_2MnSiO_4 polymorphs was first reported by Mali et al. [30] with three different polymorphs ($Pmn2_1$, $Pmnb$ and $P2_1/n$) successfully isolated by varying the preparation conditions. This study, however, focussed on structural characterization and NMR spectroscopy of the three different forms. No cycling data was presented.

Manthiram et al. [44] used a microwave-assisted, hydrothermal method to synthesize Li_2MnSiO_4 at 300 °C and 30 b pressure for 25 min at 600 W. A carbon-coated sample (12 wt.% C) was prepared with the addition of 30 wt.% sucrose and calcination in Ar at 650 °C for 6 h. The powder XRD patterns were indexed in the $P2_1$ space group but no Rietveld analysis was performed to confirm this structural designation. Particles were 20 nm in diameter and agglomerated, with a layer of amorphous carbon on the surface of the agglomerates. When cycled at C/20, Li_2MnSiO_4/C delivered a high first discharge capacity of 210 mAh g^{-1} at room temperature suggesting that >1Li-ion per formula unit could be utilized reversibly (Fig. 8). As found in earlier studies, the voltage profile on charge changed after the first charge cycle suggesting a structural change. At 55 °C, there was a reduction in polarization and a higher discharge capacity on cycling (250 mAh g^{-1} on the first discharge). Capacity retention with cycling was, however, found to be poor, especially at 55 °C. After 20 cycles only 50% capacity was retained at room temperature and only 15% at 55 °C (Fig. 9). The capacity fade was attributed to the Jahn–Teller distortion of Mn^{3+} cations and the dissolution of Mn in the electrolytes, as found for Mn oxide spinels, as well as possible amorphization, although no structural analysis of charged or cycled cathodes was reported. A DSC analysis of cathodes charged to 4.7 V showed a significantly higher heat flow (1060 J g^{-1}) for $Li_{2-x}MnSiO_4$ than for similarly prepared $Li_{2-x}FeSiO_4$ (330 J g^{-1}). This was attributed to the higher content of transition metal cations in the 4+ state in the Mn compound.

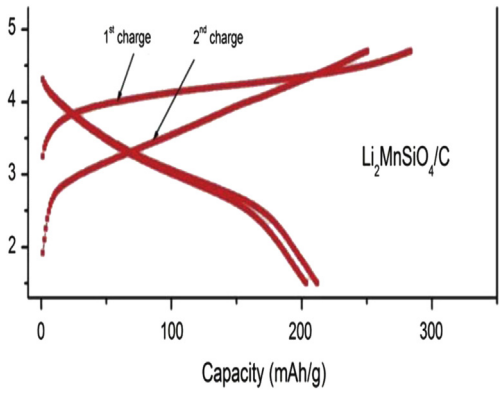

Fig. 8. Charge–discharge profiles recorded at C/20 rate and room temperature of Li_2MnSiO_4/C.
Reprinted with permission from Ref. [44]. Copyright (2010) American Chemical Society.

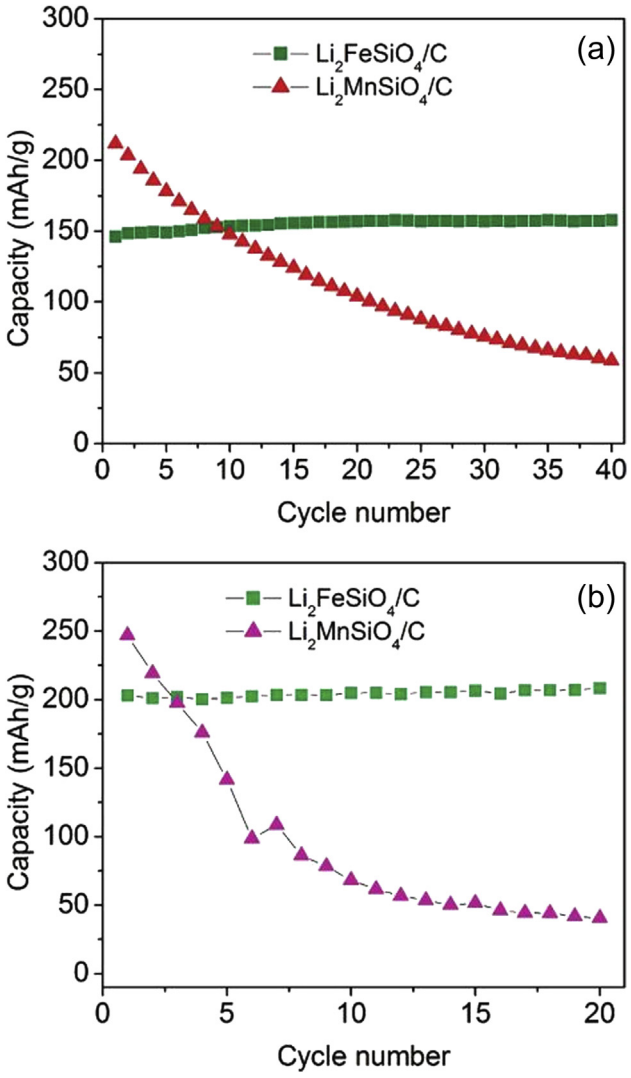

Fig. 9. Cyclability data of Li_2FeSiO_4/C and Li_2MnSiO_4/C at (a) 25 °C and (b) 55 °C.
Reprinted with permission from Ref. [44]. Copyright (2010) American Chemical Society.

Microwave-assisted solvothermal synthesis of Li_2MnSiO_4 was also reported by Kuezma et al. [45] using microwave irradiation of $LiOH \cdot H_2O$, $Mn(CH_3COO)_2 \cdot 4H_2O$ and tetraethyl orthosilicate (TEOS) with urea as catalyst in ethylene glycol at 1000 W for 2 h at 260 °C. After washing, glucono-1,5-lactone or citric acid was added and the mixed product was calcined at 700 °C for 5 h. The XRD patterns of the products showed broad peaks. The as-prepared sample was indexed as the $Pmn2_1$ polymorph while the 2 carbon-coated samples were indexed in the $P2_1/n$ space group. No detailed Rietveld refinement was reported and further structural analysis is required to confirm these structural designations especially as some characteristic reflections of the assigned polymorphs are absent in the reported XRD patterns. In particular the characteristic peaks of the $P2_1/n$ polymorph for $21 \leq 2\theta \leq 23$ (see Fig. 2) were not present for the carbon-coated samples. Particles sizes were of the order of 15–100 nm for carbon-coated samples as determined from SEM and TEM images. The best electrochemical results were reported for high citric acid content which gave a C-loading of 31.7 wt.% and resulted in first discharge capacities of 130 mAh g^{-1} at room temperature and 260 mAh g^{-1} at 50 °C with an extended voltage plateau at ~2.7 V (Fig. 10). The polarization (difference between the charge and discharge voltages) was much larger for the samples

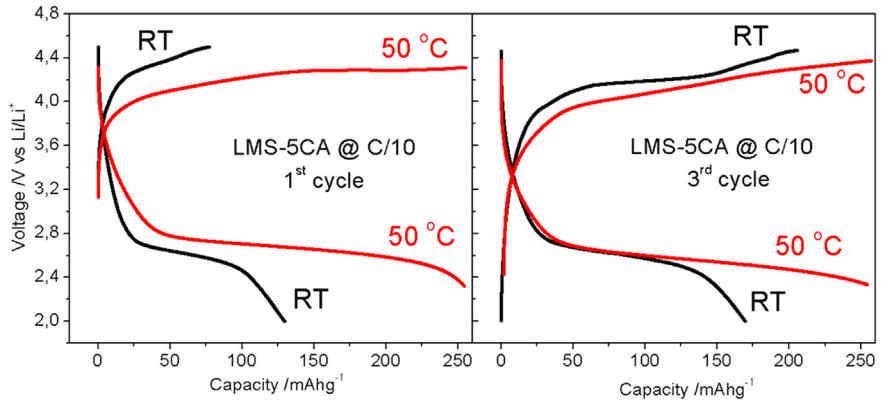

Fig. 10. Electrochemical performance for LMS-5CA at room temperature (black curve) and at elevated temperature 50 °C (red curve). (For interpretation of the references to colour in this figure legend, the reader is referred to the web version of this article.)
Reproduced from Ref. [45] with permission of The Royal Society of Chemistry.

in this study than for previously reported samples synthesized hydrothermally. In addition, the high capacity was only observed in the first few cycles and decreased drastically after the 4th cycle. XPS data of the as-prepared, fully charged (4.8 V) and discharged (2 V) samples showed that the oxidation state of the Mn cations, at least at the surface, changed from the 2+ to the 4+ state when the sample was fully charged. This is evidence for the extraction of more than one Li per formula unit from at least some of the Mn cations in the Li_2MnSiO_4 sample when fully charged. After discharge, the Mn was reduced, although the reduction to Mn^{2+} was not complete.

Hydrothermal synthesis was also reported by Aravindan et al. [46], but, in this case, adipic acid was added as the carbon source with calcination at 700 °C to carbon coat the surface. The XRD pattern was indexed in the $Pmn2_1$ space group with minor impurities of Li_2SiO_3 (before heat-treatment) and MnO (after heat-treatment). SEM micrographs showed a flower-like morphology of agglomerated nanoparticles. The material, after calcination at 700 °C, cycled reversibly in half-cells at C/20 with a capacity of 100 mAh g^{-1} for 40 cycles. It should be noted, however, that these electrodes were assembled with a ratio of almost 1:1 active material:ketjen black. This is impractical in applications as it would severely reduce the volumetric energy density of the cathodes. Further, no XRD analysis of cycled cathodes was performed so it is not known if the crystallinity of the samples was retained with cycling.

3.6. Molten carbonate flux synthesis

Kojima et al. [47] reported the use of a molten carbonate flux method for the production of single phase Li_2MnSiO_4. Single-phase products which were refined in the $Pmn2_1$ space group symmetry were produced using either $MnC_2O_4 \cdot 2H_2O$ or $Mn(OH)_2$ with Li_2SiO_3 and $(Li_{0.435}Na_{0.315}K_{0.25})_2CO_3$ under CO_2/H_2 100:3 v/v at 500–650 °C indicating that this method could significantly lower the synthesis temperature required to produce single phase material compared to other techniques such as sol–gel or solid state synthesis. The nature of the manganese precursor was found to affect the morphology of the product phase calcined at 500 °C; a sample prepared from manganese oxalate had aggregated flake-like particles with particle size of 200–600 nm, whereas the sample prepared from $Mn(OH)_2$ consisted of needle like particles with a size of 100–300 nm. The electrochemical performance of the two samples (Fig. 11) reflected this difference in morphology, with the $Mn(OH)_2$ sample giving 50% higher initial discharge capacity of 156 mAh g^{-1} compared with 96 mAh g^{-1} for the sample prepared from manganese oxalate precursors with capacity retention of 55% and 37% respectively after 20 cycles. It should be noted that, to compensate for the very low conductivity of Li_2MnSiO_4, 40 wt.% acetylene black was used in the preparation of the electrodes in this study.

3.7. Methods that fine-tune morphology for optimal performance

Using a supercritical solvothermal method, Kempaiah et al. [48] successfully prepared single phase Li_2MnSiO_4 with the $Pmn2_1$ structural form. Synthesis was performed at the low temperature of 300 °C and elevated pressure (38 MPa). After ball-milling with a conductive polymer (PEDOT), the sample was heated to 300 °C in Ar/H_2 and vacuum dried at 100 °C. The product consisted of monodisperse spherical particles 5–20 nm in diameter with 13 wt.% carbon coating (determined by TGA) (Fig. 12). The capacities reported for charging and discharging electrochemical cells were excellent, approaching the theoretical 2e capacity of

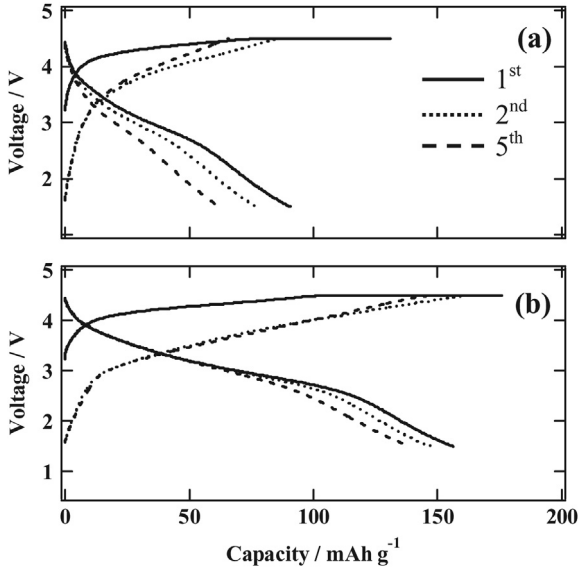

Fig. 11. Charge–discharge curves of the Li_2MnSiO_4 synthesized from (a) $MnC_2O_4 \cdot 2H_2O$ (LMS–MCO) and (b) manganese hydroxide (LMS–MOH) at 30 °C with a current density of 10 mA g^{-1} in the voltage range of 1.5–4.5 V.
Reproduced from Ref. [47] by permission of The Electrochemical Society.

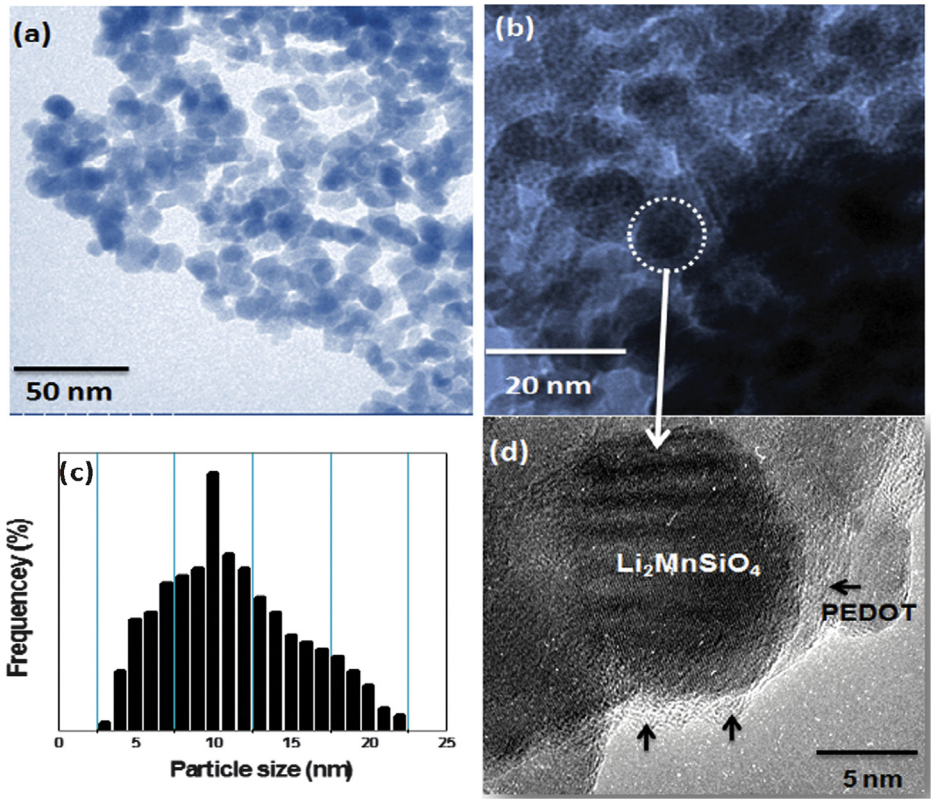

Fig. 12. (a) and (b) TEM and HRTEM images of as-synthesized Li_2MnSiO_4 and PEDOT/Li_2MnSiO_4 nanoparticles, (c) particle size distribution and (d) HRTEM image showing PEDOT-coated Li_2MnSiO_4 nanoparticles.
Reproduced from Ref. [48] with permission of The Royal Society of Chemistry.

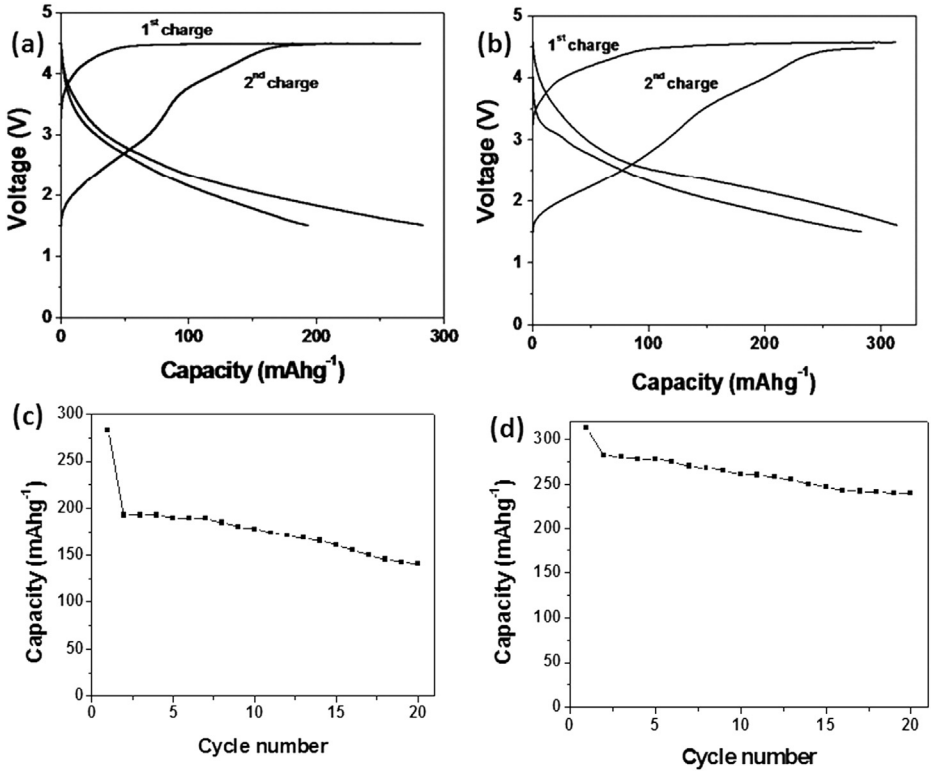

Fig. 13. Charge–discharge profiles (a and b) and cyclic performance (c and d) of PEDOT/Li_2MnSiO_4 nanoparticles recorded at C/20 in room temperature (a and c) and at 40 °C (b and d), respectively.
Reprinted from Ref. [48] with permission of The Royal Society of Chemistry.

333 mAh g^{-1}. It should be noted that, contrary to expectation, XPS data of cathodes charged to 4.5 V show a large proportion of Mn^{3+}. This suggests that much of the recorded charge capacity may be due to side reactions and electrolyte decomposition rather than to lithium extraction. The discharge curves at room temperature showed large polarization and a steeply sloping discharge curve with only about 80 mAh g^{-1} capacity above 2.5 V on the first discharge cycle and no clear plateau region in the discharge curve (Fig. 13). Although the polarization was reduced slightly at 40 °C, no significant plateau was observed above 2.5 V with only 180 mAh g^{-1} capacity observed above 2.5 V.

Kawase et al. [49] reported the use of a mesoporous carbon matrix (CMK-3 and CMK-8) with particles of Li_2MnSiO_4 deposited in the mesopores as a means to enhance the electronic conductivity of the composite cathode material. Examination of the XRD patterns of these materials (Supplementary information [49]) show that the samples contained major impurities of MnO and the peaks attributed to Li_2MnSiO_4 are very poorly defined. Galvanostatic cycling curves were recorded at 0.1C (60 mA g^{-1}) for samples with various loadings of active material in the carbon matrix. Although discharge capacities of up to 400 mAh g^{-1} were reported, the lower limit of the voltage range for the cell-cycling was 1.0 V with up to 40% of the reported capacity below 1.5 V. It is considered unlikely that the observed capacity below 1.5 V can be attributed to lithium insertion into Li_2MnSiO_4.

Nanosheet morphology has attracted much attention because of the unique properties of materials like graphene. It was also expected that this morphology would help to overcome the problems of lattice instability as a result of structural and volume change, and also enhance kinetics because of the very short lithium ion diffusion distances. Rangappa et al. [50] used a supercritical fluid technique to produce samples that consisted primarily of nanosheets of Li_2MnSiO_4 several atoms thick and with lateral dimensions of 100–300 nm. The XRD patterns of the nanosheet Li_2MnSiO_4 were assigned to the $P2_1/n$ polymorph of Li_2MnSiO_4, but several major peaks of unidentified impurity phases were present which means that the composition of the active material was not well defined. Very high capacities, initially exceeding the theoretical 2 electron capacity, were recorded for 20 cycles at 45 °C (Fig. 14). The capacity was reported to drop dramatically thereafter. XRD patterns of the cathodes, after cycling for 20 cycles, showed no peaks of the initial phase, indicating structural collapse after 20 cycles despite the nanosheet morphology.

Recent work by Devaraju et al. [51] has shown that a wide range of particle sizes and morphologies can be prepared using supercritical fluid synthesis and surfactants. After carbon coating using conducting polymers (PEDOT) and carbon black and heating to 450 °C for 5 h, the electrochemical performance of the materials was good. It should be noted, however, that the XRD patterns given for nanoparticles >30 nm in size showed major MnO impurity peaks. The results reported for hierarchical nanoparticles, in particular, showed stable high capacity over 50 cycles (240 mAh g^{-1}). Unfortunately only approximately 75 mAh g^{-1} of the discharge capacity was above 2.5 V making it very unlikely that all the discharge capacity was due to Li ion insertion (Fig. 15).

Zhao et al. [52] have reported long cycle life for 20–60 nm Li_2MnSiO_4 cathode particles coated with carbon and distributed on reduced graphene oxide networks. Synthesis was performed using a reduced graphene oxide–SiO_2 composite as a template and combining the template with lithium acetate dehydrate, manganese acetate tetrahydrate and citric acid, as a carbon source, in aqueous solution. After drying and grinding, the mixture was calcined at 400 °C for 3 h, followed by 800 °C for 10 h in Argon and produced a Li_2MnSiO_4 product ($Pmn2_1$ form) with a minor MnO impurity. At low current rates (0.05C) the discharge capacity was reported to be 290 mAh g^{-1} between 4.7 and 1.5 V, with about 140 mAh g^{-1} recorded above 2.5 V. High rate performance of ~150 mAh g^{-1} at 1C was reported with good capacity retention for 700 cycles [52].

In summary, although recent studies of nanostructured samples have produced high capacities, there remain some concerns with these results. In many cases, the Li_2MnSiO_4 phase that was believed to be responsible for the observed electrochemical capacity, was not well-defined in the experimental XRD patterns (see, for example, Fig. 16) and other, unidentified major impurity phases were also present. Further detailed structural analysis of these materials is required to fully identify the electrochemically active species. Another major concern is the very large polarization observed in the electrochemical cycling data (i.e. the large voltage difference between charge and discharge voltage). In several cases the discharge voltage dropped very steeply with increasing capacity with the average discharge voltage well below 2.5 V. Additionally, although large capacities were recorded initially, there was typically a very rapid drop in capacity after the first few cycles (Fig. 16).

3.8. Partial substitution of Fe cations for Mn

DFT calculations indicated that, although, Li_2MnSiO_4 structures ($Pmn2_1$ structural form) were predicted to collapse when Li was extracted, the substituted compounds with general formula $Li_2Mn_{0.5}Fe_{0.5}SiO_4$ were predicted to remain stable for the

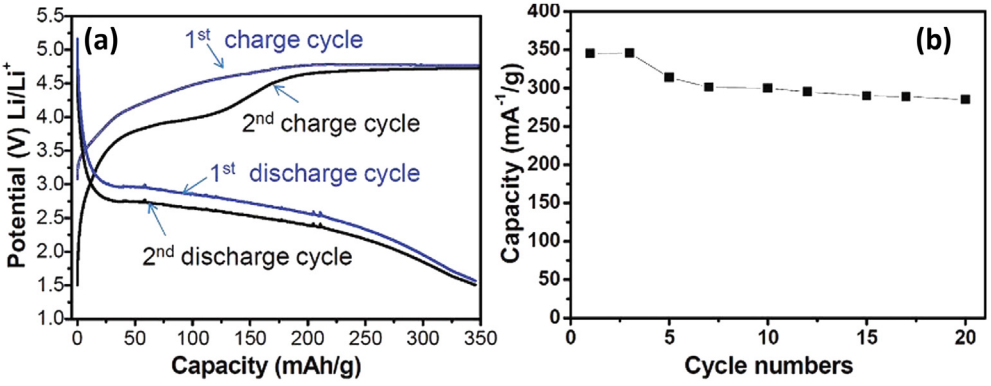

Fig. 14. Charge and discharge profile of first and second cycles. (a) Li_2MnSiO_4 samples measured at 45 °C temperatures at 0.02C rates. (b) The cyclic performance of Li_2MnSiO_4 samples.
Reprinted with permission from Ref. [50]. Copyright (2012) American Chemical Society.

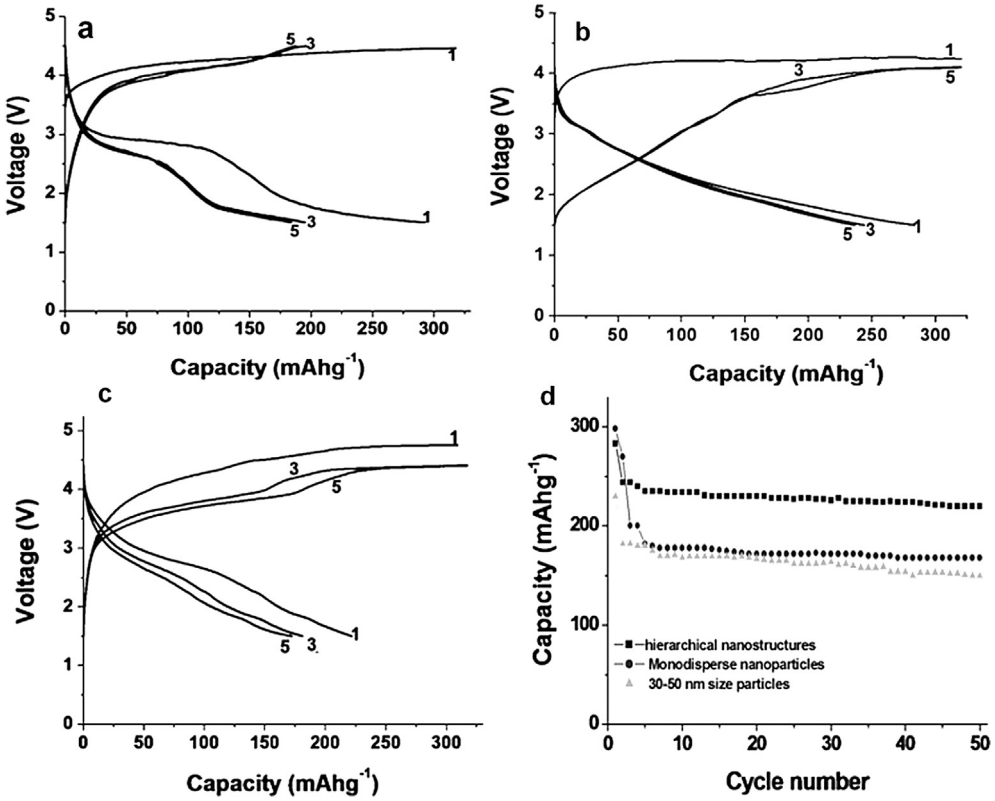

Fig. 15. Charge–discharge characteristics of Li_2MnSiO_4 positive electrode materials and cycle performance measured at room temperature with 0.05 C. (a) Charge–discharge curves of monodisperse nanoparticles showing typical 2-step discharge profiles, (b) charge–discharge curves of hierarchical nanostructures showing a gentle slope-like discharge profile and nearly two lithium ion capacity for the first cycle and more than one lithium capacity for the 3rd and 5th cycles, (c) charge–discharge curves of 30–50 nm sized particles, with more than one lithium capacity for the 1st and 3rd cycles and nearly one lithium ion capacity for the 5th cycle, and (d) the cycle performance. The hierarchical nanostructures showed excellent cycling performance with a stable capacity up to 50 cycles; monodisperse particles showed a decrease in cycle performance after a few cycles due to detachment from the carbon source; 30–50 nm sized particles showed decent cycle performance.
Reprinted from Ref. [51] with permission of The Royal Society of Chemistry.

extraction of up to 1.5Li atoms per formula unit [34]. Partial Fe substitution for Mn was therefore proposed as a possible route to improve the stability of Li_2MnSiO_4. Solid solutions with general formula $Li_2(Fe_{1-x}Mn_x)SiO_4$ (x = 0.3, 0.5, 0.7, 1) were formed by Deng [53]. It was found that Mn substitution into Li_2FeSiO_4 resulted in higher redox potentials than in pure Li_2FeSiO_4 and a slightly larger first discharge capacity, but the electrochemical reversibility and cycle stability was inferior to pure Li_2FeSiO_4, although better than that of pure Li_2MnSiO_4. The maximum reported discharge capacity for $Li_2Mn_{0.5}Fe_{0.5}O_4$ was 165 mAh g^{-1} for the first discharge and this dropped to 86 mAh g^{-1} after 50 cycles. Similar poor reversibility for $Li_2Mn_{0.5}Fe_{0.5}O_4$ and $Li_2Mn_{0.2}Fe_{0.8}O_4$ has recently been observed by Chen et al. and attributed to the instability of the Mn^{3+} cations [54].

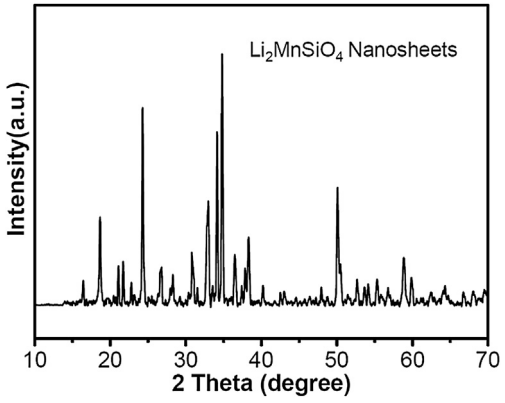

Fig. 16. XRD pattern of Li_2MnSiO_4 sample synthesized by supercritical fluid process at 400 °C temperature for 10 min reaction time.
Reprinted with permission from Ref. [50]. Copyright (2012) American Chemical Society.

4. Conclusions and future prospects

Li_2MnSiO_4 remains an attractive cathode material due to its low cost, environmentally friendly components and high theoretical capacity. Most studies to date have focussed on the $Pmn2_1$ polymorph of Li_2MnSiO_4 (Table 2) even though this form suffers structural collapse when Li is extracted. Studies using sol–gel synthesis [19,20,33,38,39,55] and molten carbonate flux synthesis [47] to prepare well-defined Li_2MnSiO_4 ($Pmn2_1$ polymorph) consistently showed initial room temperature discharge capacities of approximately 120–155 mAh g^{-1} (equivalent to insertion of approximately 0.7–0.8Li's per formula unit) at ~C/20 with rapid capacity decay with cycling. The best capacity retention after 10 cycles was shown by the carbon-coated samples of Belharouak et al. [39] (89% after 10 cycles). In contrast, well-defined Li_2MnSiO_4 ($Pmn2_1$ polymorph) samples prepared by a solution route [37] and by spray pyrolysis followed by wet ball milling [56] gave discharge capacities showing insertion of more than 1Li per formula unit (210 mAh g^{-1} for the first discharge capacity at 5 mA g^{-1} (0.03C) [37] and 200 mAh g^{-1} at 0.05C = C/20 [56] corresponding to ~1.3Li's). Consistent with other reports, the

capacity retention was poor and the samples amorphized with cycling.

Some attempts to deliberately explore other structural forms of Li_2MnSiO_4 have been made [28,29,31,32,43], but, so far, these polymorphs have shown poor electrochemical performance, comparable to, or worse than, the $Pmn2_1$ form. In most cases, however, the particle size and carbon coating has not been optimized for electrochemical performance. Further study of other polymorphs is required to fully determine the effect of structural form on electrochemical properties and structural stability with delithiation.

The hydrothermal and microwave hydrothermal synthesis techniques have shown the most success in producing samples with high electrochemical capacities [44,48] (Table 3). In several cases the phases formed have been assigned to polymorphs of Li_2MnSiO_4 different to $Pmn2_1$ such as $P2_1$ [44] and $P2_1/n$ [45,50] but these structural assignments need confirmation with detailed crystallographic studies. Further understanding of the electrochemically active species responsible for these high capacities is needed, as well as an understanding of the mechanisms responsible for the catastrophic loss of electrochemical capacity observed in some samples after cycling. It should also be noted that, in many cases (see Table 3), much of the reported capacity occurs at low voltage (<2.5 V) which would lower the overall energy density of the cathode. For example, if we calculate the gravimetric energy density of the best performing Li_2MnSiO_4 cathode from the data of Devaraju et al. (hierarchical nanoparticles) [51] with a voltage of ~2.2 V at 50% of the discharge capacity, we obtain a value of ~450 Wh kg^{-1} for the gravimetric energy density, and ~550 Wh kg^{-1} for the room temperature data of Manthiram et al. [44] with a voltage at 50% of the discharge capacity of ~3.0 V. This can be compared with the values of 560 Wh kg^{-1} for $LiFePO_4$ and 500 Wh kg^{-1} for $LiCoO_2$. The lower value obtained for the sample from the study of Devaraju et al. [51] is a consequence of the lower average voltage compared with the data of Manthiram et al. [44]. When the volumetric energy density is calculated, using the true density for each compound, the value obtained for Li_2MnSiO_4 is a relatively low 1420 Wh l^{-1} and 1730 Wh l^{-1} for the data of Devaraju et al. [51] and Manthiram et al. [44], respectively, compared to $LiFePO_4$ (2000 Wh l^{-1}) and $LiCoO_2$ (2600 Wh l^{-1}). The gravimetric energy density of Li_2MnSiO_4 samples can therefore be competitive with other commonly used materials. The relatively low volumetric energy density values are a consequence of the low density of the material of 3.15 g cm^{-3} (for the $Pmn2_1$ polymorph).

To date results for $Li_2(Fe_{1-x}Mn_x)SiO_4$ samples have been disappointing, but mixed transition metal silicates still offer a rich area for potential future exploration analogous to the mixed transition metal oxides such as $LiNi_{1/3}Mn_{1/3}Co_{1/3}O_2$, that have been optimized to improve battery cathode performance [18]. Recent DFT calculations have shown the potential of the multicomponent $Li_2Mn_{1/3}Fe_{1/3}Ni_{1/3}SiO_4$, for example, with predicted extraction voltages for both the 1st and 2nd lithium ions at around 4.2 V, and a reduced band gap compared to single component systems, which should lead to higher electronic conductivity [54]. The calculations, however, also predict that structural changes will occur with lithium extraction from this multicomponent silicate, as found in the single component systems. It remains to be seen if synthesis of this material is feasible and whether structural changes compromise the electrochemical performance.

Improvements in the electrochemical performance of Li_2MnSiO_4 cathodes have been reported recently, but reliable performance, over many cycles, remains to be achieved. Stabilization of the Li_2MnSiO_4 structure when Li is extracted is required, and interactions with the electrolyte need to be minimized. In recent years, novel synthesis methods have been developed to engineer the particle size, morphology and carbon-coating, but further work is required to clearly define the chemical composition and the structure of the active material in the electrodes, and to provide well-defined, reliable, high-performance materials.

Appendix A. Supplementary data

Supplementary data related to this article can be found at http://dx.doi.org/10.1016/j.jpowsour.2013.11.082.

References

[1] T. Nagaura, K. Tozawa, Prog. Batteries Sol. Cells 9 (1990) 209.
[2] C. Daniel, JOM – US 60 (2008) 43–48.
[3] M.M. Thackeray, C. Wolverton, E.D. Isaacs, Energy Environ. Sci. 5 (2012) 7854–7863.
[4] T. Xu, W. Wang, M.L. Gordin, D.H. Wang, D.W. Choi, JOM – US 62 (2010) 24–30.
[5] K. Mizushima, P.C. Jones, P.J. Wiseman, J.B. Goodenough, Mater. Res. Bull. 15 (1980) 783–789.
[6] D. Doughty, E.P. Roth, Electrochem. Soc. Interfaces (2012) 37–44.
[7] T. Ohzuku, Y. Makimura, Chem. Lett. (2001) 642–643.
[8] N. Yabuuchi, T. Ohzuku, J. Power Sources 146 (2005) 636–639.
[9] M. Armand, World Patent WO02/27823, 2002.
[10] A.K. Padhi, K.S. Nanjundaswamy, J.B. Goodenough, J. Electrochem. Soc. 144 (1997) 1188–1194.
[11] M.E. Arroyo-de Dompablo, M. Armand, J.M. Tarascon, U. Amador, Electrochem. Commun. 8 (2006) 1292–1298.
[12] A.K. Padhi, K.S. Nanjundaswamy, C. Masquelier, S. Okada, J.B. Goodenough, J. Electrochem. Soc. 144 (1997) 1609–1613.
[13] A. Yamada, S.C. Chung, K. Hinokuma, J. Electrochem. Soc. 148 (2001) A224–A229.
[14] S.Y. Chung, J.T. Bloking, Y.M. Chiang, Nat. Mater. 1 (2002) 123–128.
[15] N. Ravet, Y. Chouinard, J.F. Magnan, S. Besner, M. Gauthier, M. Armand, J. Power Sources 97–98 (2001) 503–507.
[16] H. Huang, S.C. Yin, L.F. Nazar, Electrochem. Solid State Lett. 4 (2001) A170–A172.
[17] B. Kang, G. Ceder, Nature 458 (2009) 190–193.
[18] M.S. Islam, R. Dominko, C. Masquelier, C. Sirisopanaporn, A.R. Armstrong, P.G. Bruce, J. Mater. Chem. 21 (2011) 9811–9818.
[19] R. Dominko, M. Bele, M. Gaberscek, A. Meden, M. Remskar, J. Jamnik, Electrochem. Commun. 8 (2) (2006) 217–222.
[20] R. Dominko, M. Bele, A. Kokalj, M. Gaberscek, J. Jamnik, J. Power Sources 174 (2007) 457–461.
[21] A.R. West, F.P. Glasser, J. Solid State Chem. 4 (1972) 20.
[22] T. Ohzuku, A. Ueda, N. Yamamoto, J. Electrochem. Soc. 142 (1995) 1431–1435.
[23] C. Sirisopanaporn, C. Masquelier, P.G. Bruce, A.R. Armstrong, R. Dominko, J. Am. Chem. Soc. 133 (2011) 1263–1265.
[24] A. Nyten, S. Kamali, L. Haggstrom, T. Gustafsson, J.O. Thomas, J. Mater. Chem. 16 (2006) 2266–2272.
[25] A. Nyten, A. Abouimrane, M. Armand, T. Gustafsson, J.O. Thomas, Electrochem. Commun. 7 (2005) 156–160.
[26] M. Sato, T. Ishigaki, K. Uematsu, K. Toda, H. Okawa, Acta Crystallogr., Sect. E 68 (2012) i68–i69.
[27] M.E. Arroyo-deDompablo, R. Dominko, J.M. Gallardo-Amores, L. Dupont, G. Mali, H. Ehrenberg, J. Jamnik, E. Moran, Chem. Mater. 20 (2008) 5574–5584.
[28] R.J. Gummow, N. Sharma, V.K. Peterson, Y. He, J. Solid State Chem. 188C (2012) 32–37.
[29] V.V. Politaev, A.A. Petrenko, V.B. Nalbandyan, B.S. Medvedev, E.S. Shvetsova, J. Solid State Chem. 180 (2007) 1045–1050.
[30] G. Mali, A. Meden, R. Dominko, Chem. Commun. 46 (2010) 3306–3308.
[31] R.J. Gummow, N. Sharma, V.K. Peterson, Y. He, J. Power Sources 197 (2012) 231–237.
[32] H. Duncan, A. Kondamreddy, P.H.J. Mercier, Y. Le Page, Y. Abu-Lebdeh, M. Couillard, P.S. Whitfield, I.J. Davidson, Chem. Mater. 23 (2011) 5446–5456.
[33] R. Dominko, J. Power Sources 184 (2008) 462–468.
[34] A. Kokalj, R. Dominko, G. Mali, A. Meden, M. Gaberscek, J. Jamnik, Chem. Mater. 19 (2007) 3633–3640.
[35] N. Kuganathan, M.S. Islam, Chem. Mater. 21 (2009) 5196–5202.
[36] C.A.J. Fisher, N. Kuganathan, M.S. Islam, J. Mater. Chem. A 1 (2013) 4207–4214.
[37] Y.X. Li, Z.L. Gong, Y. Yang, J. Power Sources 174 (2007) 528–532.
[38] C. Deng, S. Zhang, B.L. Fu, S.Y. Yang, L. Ma, Mater. Chem. Phys. 120 (2010) 14–17.
[39] I. Belharouak, A. Abouimrane, K. Amine, J. Phys. Chem. C 113 (2009) 20733–20737.

[40] V. Aravindan, K. Karthikeyan, S. Ravi, S. Amaresh, W.S. Kim, Y.S. Lee, J. Mater. Chem. 20 (2010) 7340–7343.
[41] R. Dominko, I. Arcon, A. Kodre, D. Hanzel, M. Gaberscek, J. Power Sources 189 (2009) 51–58.
[42] V. Aravindan, K. Karthikeyan, K.S. Kang, W.S. Yoon, W.S. Kim, Y.S. Lee, J. Mater. Chem. 21 (2011) 2470–2475.
[43] R.J. Gummow, M.G. Blackford, G.R. Lumpkin, Y. He, J. Alloys Compd. 551 (2013) 521–526.
[44] A. Manthiram, T. Muraliganth, K.R. Stroukoff, Chem. Mater. 22 (2010) 5754–5761.
[45] M. Kuezma, S. Devaraj, P. Balaya, J. Mater. Chem. 22 (2012) 21279–21284.
[46] V. Aravindan, K. Karthikeyan, J.W. Lee, S. Madhavi, Y.S. Lee, J. Phys. D Appl. Phys. 44 (2011) 152001.
[47] A. Kojima, T. Kojima, M. Tabuchi, T. Sakai, J. Electrochem. Soc. 159 (2012) A532–A537.
[48] D.M. Kempaiah, D. Rangappa, I. Honma, Chem. Commun. 48 (2012) 2698–2700.
[49] T. Kawase, H. Yoshitake, Micropor. Mesopor. Mater. 155 (2012) 99–105.
[50] D. Rangappa, K.D. Murukanahally, T. Tomai, A. Unemoto, I. Honma, Nano Lett. 12 (2012) 1146–1151.
[51] M.K. Devaraju, T. Tomai, A. Unemoto, I. Honma, RSC Adv. 3 (2013) 608–615.
[52] Y. Zhao, C. Wu, J. Li, L. Guan, J. Mater. Chem. A 1 (2013) 3856–3859.
[53] C. Deng, S. Zhang, S.Y. Yang, J. Alloys Compd. 487 (2009) L18–L23.
[54] R.Y. Chen, R. Heinzmann, S. Mangold, V.S.K. Chakravadhanula, H. Hahn, S. Indris, J. Phys. Chem. C 117 (2013) 884–893.
[55] W.G. Liu, Y.H. Xu, R. Yang, Rare Metals 29 (2010) 511–514.
[56] B. Shao, Y. Abe, I. Taniguchi, Powder Technol. 235 (2013) 1–8.